JPL Publication 89-9

A Doppler Centroid Estimation Algorithm for SAR Systems Optimized for the Quasi-Homogeneous Source

Michael Y. Jin

October 1, 1989

National Aeronautics and Space Administration

Jet Propulsion Laboratory
California Institute of Technology
Pasadena, California

TECHNICAL REPORT STANDARD TITLE PAGE

1. Report No. 89-9	2. Government Accession No.	3. Recipient's Catalog No.
4. Title and Subtitle A Doppler Centroid Estimation Algorithm for SAR Systems Optimized for the Quasi-Homogeneous Source		5. Report Date October 1, 1989 6. Performing Organization Code
7. Author(s) Michael Y. Jin		8. Performing Organization Report No.
9. Performing Organization Name and Address JET PROPULSION LABORATORY California Institute of Technology 4800 Oak Grove Drive Pasadena, California 91109		10. Work Unit No. 11. Contract or Grant No. NAS7-918 13. Type of Report and Period Covered JPL Publication
12. Sponsoring Agency Name and Address NATIONAL AERONAUTICS AND SPACE ADMINISTRATION Washington, D.C. 20546		14. Sponsoring Agency Code RE 215 BP-889-62-50-37-01

15. Supplementary Notes

16. Abstract Radar signal processing applications frequently require an estimate of the Doppler centroid of a received signal. The Doppler centroid estimate is required for synthetic-aperture radar (SAR) processing. It is also required for some applications involving target-motion estimation and antenna pointing direction estimation. In some cases, the Doppler centroid can be accurately estimated based on available information regarding the terrain topography, the relative motion between the sensor and the terrain, and the antenna pointing direction. Often, the accuracy of the Doppler centroid estimate can be improved by analyzing the characteristics of the received SAR signal. This kind of signal processing is also referred to as clutterlock processing. This publication reports on a Doppler centroid estimation (DCE) algorithm which contains a linear estimator optimized for the type of terrain surface that can be modeled by a quasi-homogeneous source.

Information on the following topics is presented in this publication:

- o an introduction to the theory of Doppler centroid estimation
- o analysis of the performance characteristics of previously reported DCE algorithms
- o comparison of these analysis results with experimental results
- o a description and performance analysis of a Doppler centroid estimator which is optimized for a QHS
- o comparison of the performance of the optimal QHS Doppler centroid estimator with that of previously reported methods

17. Key Words (Selected by Author(s))	18. Distribution Statement
Statistics and Probability Radar Detection	Unclassified; unlimited

19. Security Classif. (of this report)	20. Security Classif. (of this page)	21. No. of Pages	22. Price
Unclassified	Unclassified	50	

JPL Publication 89-9

A Doppler Centroid Estimation Algorithm for SAR Systems Optimized for the Quasi-Homogeneous Source

Michael Y. Jin

October 1, 1989

National Aeronautics and
Space Administration

Jet Propulsion Laboratory
California Institute of Technology
Pasadena, California

The research described in this publication was carried out by the Jet Propulsion Laboratory, California Institute of Technology, under a contract with the National Aeronautics and Space Administration.

ABSTRACT

Radar signal processing applications frequently require an estimate of the Doppler centroid of a received signal. The Doppler centroid estimate is required for synthetic-aperture radar (SAR) processing. It is also required for some applications involving target-motion estimation and antenna pointing direction estimation. In some cases, the Doppler centroid can be accurately estimated based on available information regarding the terrain topography, the relative motion between the sensor and the terrain, and the antenna pointing direction. Often, the accuracy of the Doppler centroid estimate can be improved by analyzing the characteristics of the received SAR signal. This kind of signal processing is also referred to as clutterlock processing. This publication reports on a Doppler centroid estimation (DCE) algorithm which contains a linear estimator optimized for the type of terrain surface that can be modeled by a quasi-homogeneous source (QHS).

Information on the following topics is presented in this publication:

- an introduction to the theory of Doppler centroid estimation
- analysis of the performance characteristics of previously reported DCE algorithms
- comparison of these analysis results with experimental results
- a description and performance analysis of a Doppler centroid estimator which is optimized for a QHS
- comparison of the performance of the optimal QHS Doppler centroid estimator with that of previously reported methods

ACKNOWLEDGEMENT

The author wishes to thank R. Piereson and K. Leung for carefully reviewing this manuscript.

TABLE OF CONTENTS

I. INTRODUCTION 1-1

II. DOPPLER CENTROID ESTIMATION FROM SAR DATA 2-1

A. POINT-TARGET SAR ECHO RESPONSE 2-1

B. DISTRIBUTED-TARGET RESPONSE 2-2

Algorithm I. (Li et al.)..... 2-4

Algorithm II. (Curlander et al.)..... 2-4

Algorithm III. 2-5

III. PERFORMANCE ANALYSIS OF DCE ALGORITHM III 3-1

A. SAR IMPULSE RESPONSES OF INDEPENDENT LOOKS 3-1

B. TARGET MODEL 3-4

C. PDF OF THE ENERGY OF A SINGLE-LOOK IMAGE..... 3-5

D. PDF OF THE NORMALIZED ENERGY DIFFERENCE 3-7

E. STANDARD DEVIATION OF THE DOPPLER CENTROID ESTIMATE 3-10

F. AZIMUTH AMBIGUITY EFFECT 3-12

G. SYSTEM-NOISE EFFECT ON DOPPLER ESTIMATION 3-14

IV. EXPERIMENTAL RESULTS: GENERALIZED DCE ALGORITHM 4-1

V. OPTIMAL DOPPLER CENTROID ESTIMATION FOR QHS 5-1

A. OPTIMAL DOPPLER CENTROID ESTIMATION FOR HS 5-3

VI. EXPERIMENTAL RESULTS: OPTIMAL QHS-DCE ALGORITHM 6-1

VII. CONCLUSION 7-1

VIII. APPENDICES

A. PROOF OF (23) AND PROOF OF (24) A-1

B. OPTIMAL DOPPLER CENTROID ESTIMATION FOR HS B-1

C. REFERENCES C-1

Figures

1. SAR Response of a Point-Target: (a) Point-Target Echo Response in Azimuth, (b) Spectrum of Point-Target Echo Response in Magnitude 2-3

2. Doppler Centroid Estimation Approaches: (a) Algorithm I (Li et al.), (b) Algorithm II (Curlander et al.) 2-6

3. Contours and Projections of $p(\Delta f, \Delta \bar{E})$ 3-11

4. Block Diagram of an Optimal QHS-DCE Algorithm 5-5

Tables

I. Results of DCE Algorithm III and Prediction 4-2

II. Results of an Optimal QHS-DCE Algorithm 6-2

SECTION I

INTRODUCTION

The quality of SAR images strongly depends on the accuracy of the knowledge of the range history of the sensor relative to the terrain during the interval of observation. In many applications, this range (or signal phase) history can be accurately modeled by a second-order Taylor series expanded about the center of the synthetic aperture. The coefficient of the quadratic term is equal to the Doppler frequency rate. An error in this parameter causes broadening of the SAR impulse response. The coefficient of the linear term is equal to the Doppler frequency associated with a point located at the center of the antenna beam. An error in this parameter causes degradation of several image-quality factors including the signal-to-noise ratio (SNR) and the signal-to-ambiguity ratio (STAR) [1].

A SAR antenna pattern is usually symmetric with its peak gain at the center of the beam. The best SNR and STAR are obtained by selecting a processing-frequency band centered at the Doppler centroid. These image-performance factors are degraded when there is a mismatch between the center of the processing band and the Doppler centroid. In many other related applications, such as determination of the speed of moving targets [2, 3] and determination of antenna pointing direction [4], the system performance is directly affected by the accuracy of the Doppler centroid estimate. The value of developing a more accurate DCE algorithm is therefore apparent.

Doppler parameters are often computed from the sensor-target relative position, velocity, and acceleration vectors [5]. Alternatively, these

parameters can be estimated from the SAR image data, as demonstrated by Li et al. [1]. The principle of this algorithm is that the intensity profile of the range-averaged power spectrum of the image data is a function of the antenna pattern in the azimuth dimension. The peak in the spectrum corresponds to the Doppler centroid. That method was found to enable an improvement in the Doppler centroid estimate when the ephemeris data contains significant errors. Such was the case in both the Seasat and SIR-B missions. Several other methods, similar in principle, were presented by Curlander et al. [6]. However, no performance analysis of those algorithms has been published. Consequently, comparison of performances among these algorithms in the available literature lacks a theoretical basis.

In the first part of this publication, two previously reported DCE algorithms and a generalized algorithm are described. The performance analysis for this generalized algorithm is then presented. This analysis assumes that the statistical properties of the backscatter coefficients of targets follow those of a QHS. This assumption is valid for many physical sources. Hence, the result of this analysis is applicable to a large percentage of the SAR data. Experimental results obtained using Seasat and SIR-B data agree well with the analysis.

One fact observed from the result of the performance analysis with a QHS is that the error of the Doppler centroid estimate provided by the generalized algorithm increases when the contrast within the SAR image increases. This indicates that the generalized algorithm is not optimized for the QHS. Further studies showed that this algorithm is also not an optimal approach for a strictly homogeneous source (HS). This finding was the motivation for

developing an optimal DCE algorithm applicable to a wider range of terrain characteristics.

The second part of this publication describes the design of an optimal DCE process. In this design, a number of optimal Doppler centroid measures are obtained by processing a number of spatially diversed subsets of image pixels with a linear estimator; each subset is strictly homogeneous. A single final Doppler centroid estimate is then given by the average of the weighted Doppler centroid measures. These weight coefficients are generated based on the maximum likelihood criterion so as to minimize the variance of the final Doppler centroid estimate. In the special case of the homogeneous source, these weight coefficients are proportional to the number of pixels in each subset.

To demonstrate the validity of this optimal DCE algorithm and the improvement of the estimation accuracy, several Seasat and SIR-B SAR data sets were processed. Results show that the optimal DCE algorithm generally yields more accurate Doppler centroid estimates than the previous algorithms.

SECTION II

DOPPLER CENTROID ESTIMATION FROM SAR DATA

To illustrate the concept of the DCE by using SAR data, we will start with a simple case in which the SAR echo response is due to a single point-target (consisting of one scatterer with its dimension much smaller than the SAR resolution). This concept is then extended to a more general case in which the SAR echo response is contributed by a large number of distributed targets (consisting of many scatterers in one resolution cell). Previous DCE algorithms are briefly reviewed, and a generalized algorithm is then presented.

A. POINT-TARGET SAR ECHO RESPONSE

The echo response of a SAR from an isotropic point-target reflector can be modeled by its amplitude and phase variations in the along-track dimension [5], i.e.,

$$Rp(t) = W_a^{1/2}(t) \cdot \exp\{-j\phi(t)\} \tag{1}$$

where $W_a(t)$ is the azimuth antenna weighting and $\phi(t)$ is the phase history, which is a function of the sensor-target range history. The phase history can be modeled by a quadratic function, i.e.,

$$\phi(t) = 2\pi \left(f_{dc} \cdot t + \frac{1}{2} \cdot f_r \cdot t^2 \right) \tag{2}$$

where f_{dc} is the Doppler centroid and f_r is the Doppler frequency rate. For this simple case, the Doppler centroid can be determined directly from the echoes by tracing the phase-change rate at the time of the response peak. For a response with a large time-bandwidth product, the amplitude of the Fourier transform of this response takes the same form. Therefore, one can also determine the Doppler centroid in the frequency domain. The echo response and spectrum in the azimuth dimension for a point-target are illustrated in Figure 1. Note that to satisfy Eq. (1), isotropy is not an essential property of the target. An adequate and less stringent condition is that the target backscatter be independent of the azimuth angle change over the illumination period. It is believed that many types of targets exhibit this property, especially for cases with a narrow antenna beamwidth. This property will be assumed in the following analysis.

B. DISTRIBUTED-TARGET RESPONSE

In determining the Doppler centroid for a distributed target, two problems may be encountered. First, tracing the phase change for each target by analyzing the response data in the time domain is impossible because the SAR echo response is a superposition of many point-target responses. Second, fading may exist in each spectral component because of the random-phase process of the naturally occurring targets. Consequently, the Doppler centroid estimate processed from a single azimuth power spectrum exhibits significant error.

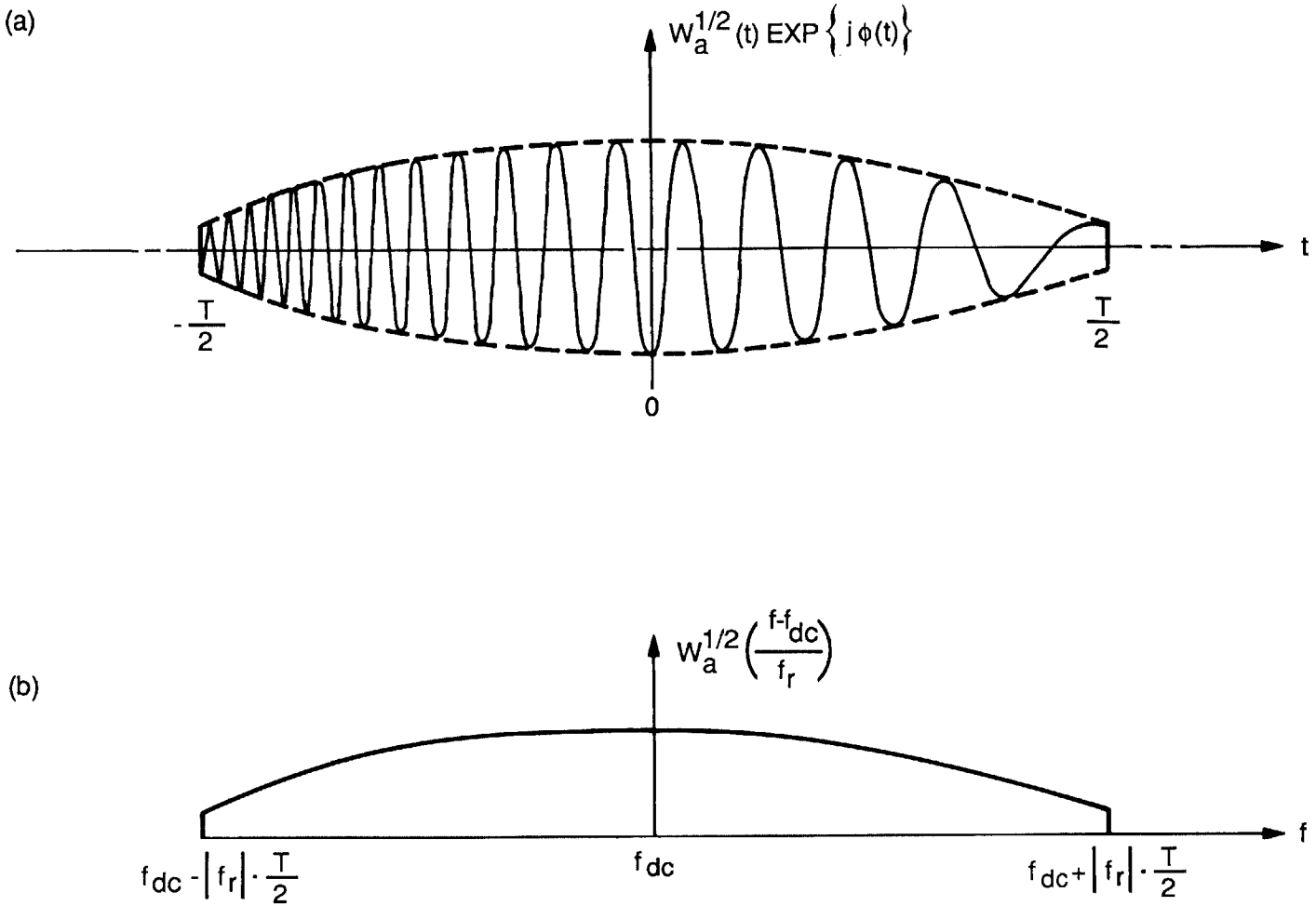

Figure 1. SAR Response of a Point-Target: (a) Point-Target Echo Response in Azimuth, (b) Spectrum of Point-Target Echo Response in Magnitude

A commonly adopted method [7] is to obtain a few azimuth power spectra from the response data, average them to improve the signal-to-noise ratio, and extract the Doppler centroid by searching for the peak of the averaged spectrum. Li [1] noted that this method usually cannot provide high accuracy and showed that a much more accurate estimate can be obtained from the range-averaged spectrum of a processed SAR image. In the following, we summarize processing procedures of algorithms given by both Li et al. and Curlander et al.

1. Algorithm I. (Li et al.)

Process the SAR echo response into a full-resolution image with an initially estimated Doppler centroid and an accurate Doppler frequency rate. Fourier transform this image data in the azimuth dimension and perform detection to obtain the power density for each frequency channel. Average these detected spectra along the range dimension and search for a frequency channel which has the energy on both sides balanced. Iteration of this process may be required if the initial estimate used for processing the image contains a large error.

2. Algorithm II. (Curlander et al.)

Process the SAR echo response into four independent single-look images. Each image uses one-fourth the total processing bandwidth, and the spectra of these images are consecutive. Then compute the following quantity:

$$\Delta\bar{E} = \frac{E_1 + E_2 - E_3 - E_4}{\sum_{i=1}^{4} E_i} \qquad (3)$$

where E_i denotes the total energy in the i-th look. Repeat this procedure for several selected values of the Doppler centroid. Perform linear regression for E as a fuction of the processing Doppler values. The Doppler centroid estimate is selected from the intersection of the linearly fitted line and the line of $\Delta\bar{E} = 0$.

Both of these algorithms are illustrated in Figure 2. Algorithm I described above requires processing full-resolution SAR images, which is a disadvantage if the normal processor output is multi-look (reduced-resolution) imagery. Algorithm II involves a relatively large computation load and may not be efficient. Algorithm III (described below) is a generalized DCE algorithm which was evolved from the above algorithms. The performance analysis of algorithm III can be easily made and is applicable to the above algorithms.

3. Algorithm III.

The first step of this algorithm is to process the SAR echo response into N independent single-look images, each with 1/N of the total processing bandwidth, where N is an even number and the spectra of these images are consecutive. Then the following quantity is computed:

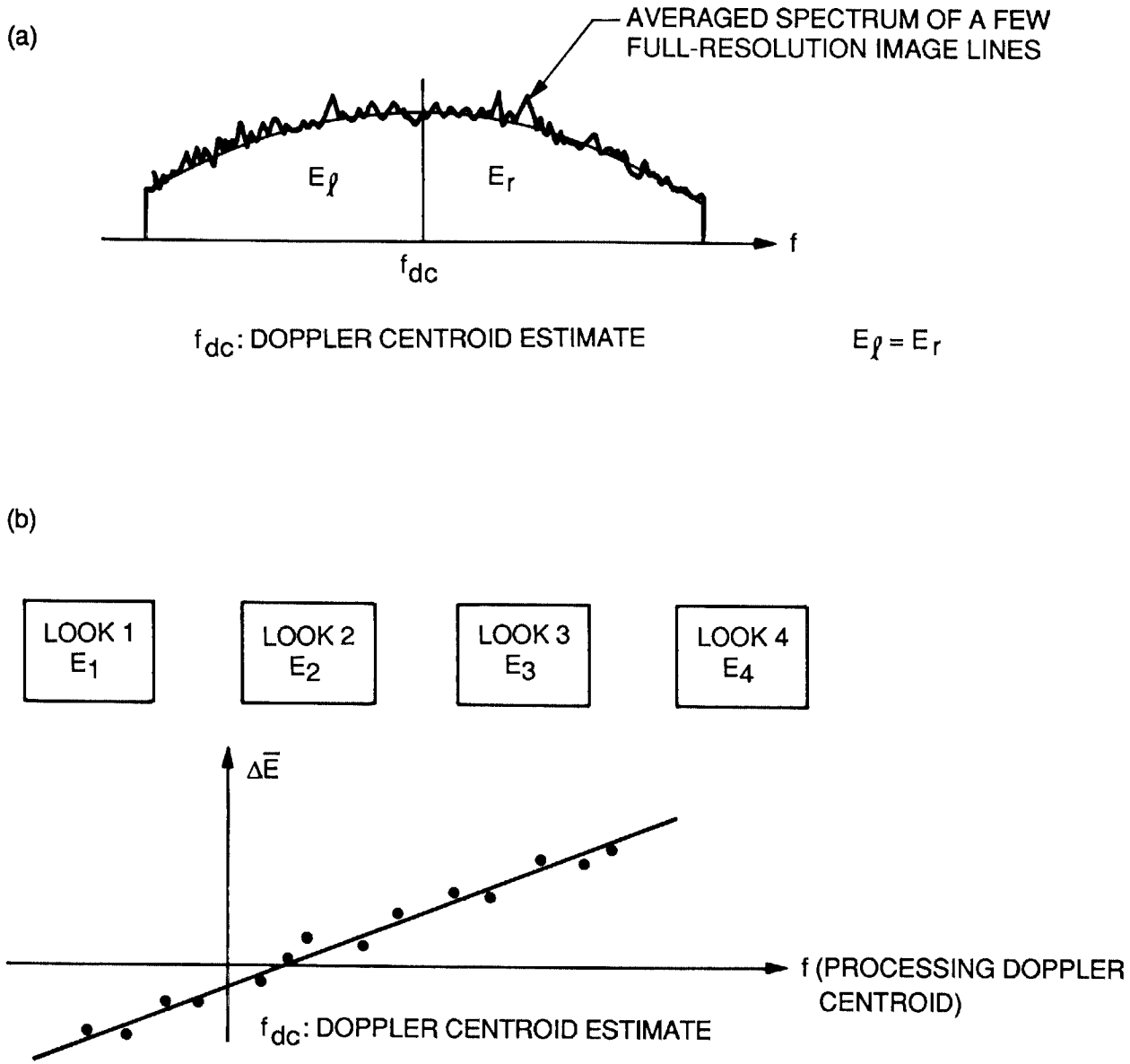

Figure 2. Doppler Centroid Estimation Approaches: (a) Algorithm I (Li et al.), (b) Algorithm II (Curlander et al.)

$$\Delta\bar{E} = \frac{\sum_{i=1}^{N/2} E_i - \sum_{i=N/2+1}^{N} E_i}{\sum_{i=1}^{N} E_i} \tag{4}$$

where E_i denotes the total energy in the i-th look. Obtain the Doppler centroid estimate by subtracting the estimated error Δf of the processing Doppler ($\Delta f = C_1^{-1} \Delta\bar{E}$, C_1 is given in Eq. (35)) from the processing Doppler. Repeat this procedure until $\Delta\bar{E}$ approaches zero.

It is obvious that this algorithm is equivalent to algorithm I when N is equal to two. With N equal to four, this algorithm is very close to algorithm II. However, there is a slight difference in the performances, which will be discussed later.

SECTION III

PERFORMANCE ANALYSIS OF DCE ALGORITHM III

In DCE algorithm III, the accuracy of the estimated Doppler centroid is determined by the statistical characteristics of the normalized energy difference $\Delta\bar{E}$. It is therefore necessary to formulate the probability density function of $\Delta\bar{E}$. This pdf is used to derive the standard deviation of the Doppler centroid estimate.

A. SAR IMPULSE RESPONSES OF INDEPENDENT LOOKS

The SAR impulse response can be expressed as the convolution of the returned point-target echo with a reference function. If there is no amplitude weighting included in the reference function, the impulse response in the azimuth dimension is given by

$$h(t) = Rp(t) \circledast \{\exp[j\phi(t)]\ \mathrm{Rect}(t/T)\} \tag{5}$$

where $\circledast$ denotes the convolution, Rp(t) is the SAR point-target response after range correlation, and Rect(.) is the rectangular function defined by

$$\mathrm{Rect}(t/T) = \begin{cases} 1 & |t| \le T/2 \\ 0 & \text{otherwise} \end{cases} \tag{6}$$

where T denotes the processing aperture width. For a mismatch between the processing Doppler centroid and the true Doppler centroid by Δf, the reference function is equivalent to the previous one having a time delay $\Delta f/f_r$, i.e.,

$$h(t,\Delta f) = Rp(t) \circledast \left\{ \exp[j\phi(t)] \right.$$
$$\left. \text{Rect} \left((t - \Delta f/f_r)/T \right) \right\} \tag{7}$$

For a reference function with a large time-bandwidth product (TBP), the magnitude of the impulse spectrum takes the same form as the antenna weighting in the time domain, i.e.,

$$\left| F\{h(t,\Delta f)\} \right| = W_a^{1/2} \left((f - f_{dc})/f_r \right)$$
$$\text{Rect} \left((f - f_{dc} - \Delta f)/PBW \right) \tag{8}$$

where PBW is the processing bandwidth given by $f_r \cdot T$. It is convenient to define

$$\hat{W}_a(f) = W_a \left((f - f_{dc})/f_r \right) \tag{9}$$

Images produced by a coherent system are corrupted by speckle noise. Methods of noncoherent averaging that reduce the speckle noise and are based upon properties of spatial or frequency diversity [8] have been reported [9,10]. The trade-off of speckle reduction is the broadening of the resolution width. In SAR, statistically independent looks can be generated from spatially separated subapertures. For the case with the total number of looks being equal to N, the impulse response corresponding to the i-th subaperture can be expressed by

$$h_i(t,\Delta f) = Rp(t) \circledast \left\{ \exp[j\phi(t)] \right.$$
$$\left. \text{Rect} \left((t - t_i - \Delta f/f_r)/(T/N) \right) \right\} \tag{10}$$

where t_i is the time delay associated with the i-th subaperture and

$$t_i = (i - 1)\ T/N - T/2 \tag{11}$$

If the TBP of each subaperture is also large, the spectrum of the i-th impulse response can be approximated by

$$\left| F\{h_i(t,\Delta f)\} \right| = \hat{W}_a^{1/2}(f)\ \text{Rect}\left((f - f_i - \Delta f)/(PBW/N) \right) \tag{12}$$

where

$$f_i = f_{dc} + f_r \cdot t_i \tag{13}$$

The following property can be derived directly from this approximation:

$$h_i(t,\Delta f) \circledast h_j(t,\Delta f) = 0 \quad \text{for } i \neq j \tag{14}$$

If the azimuth ambiguity (spectral aliasing due to limited pulse repetition frequency) makes a negligible contribution to the impulse response, the following properties can be shown to be true:

$$\sum_i \int \left| h_i(t,\Delta f) \right|^2 dt = \int_{\frac{-PBW}{2} + \Delta f}^{\frac{PBW}{2} + \Delta f} \hat{W}_a(f)\ df \tag{15}$$

and

$$\sum_i \int \left| h_i(t,\Delta f) \circledast h_i^*(t,\Delta f) \right|^2 dt = \int_{\frac{-PBW}{2}+\Delta f}^{\frac{PBW}{2}+\Delta f} \hat{W}_a^2(f)\, df \qquad (16)$$

where * denotes the complex conjugate.

B. TARGET MODEL

The concept of the quasi-homogeneous source has been brought forth by Carter and Wolf [11] to model many physical light sources and to derive coherence properties and radiometric properties of light generated by such sources.

In SAR, a similar model was used by Raney [12] to derive the SAR system-transfer function and some useful properties. With this model, the spatial waveform of the SAR target reflection can be expressed as

$$G(a) = A^{1/2}(a)\, X(a) \qquad (17)$$

where a denotes the spatial coordinates of the along-track dimension and A(a) denotes the backscatter coefficient, which is also known as the reflectivity density. A(a) is assumed to be slowly varying. X(a) is a complex random process resulting from the phase variation of the numerous small scatterers; it has dimensions comparable to the wavelength of the SAR. X(a) is assumed to

be a wide-sense stationary zero-mean complex Gaussian random process with independent quadrature components. The second and fourth moments of X are

$$e[X(a_1)\ X^*(a_2)] = \delta(a_1 - a_2) \tag{18}$$

$$e[X(a_1)\ X^*(a_2)\ X(a_3)\ X^*(a_4)] = \delta(a_1 - a_2)\ \delta(a_3 - a_4) + \delta(a_1 - a_4)\ \delta(a_2 - a_3) \tag{19}$$

where $\delta(.)$ denotes a finite-impulse response which can be approximated by the Dirac's Delta function when the SAR resolution width is much greater than the wavelength.

C. PDF OF THE ENERGY OF A SINGLE-LOOK IMAGE

In general, a stable sensor flight path is required during SAR mapping to maintain a stable sensor-target geometry and a slow drift of the Doppler centroid. This SAR requirement is meant to make the image processing a much easier task. In this case, the SAR image can be expressed as the convolution of the target waveform and the impulse response. The image generated from the i-th look, with error Δf in the processing Doppler centroid, is given by

$$G_i'(a,\Delta f) = G(a) \ \textcircled{x}\ h_i(a,\Delta f) \tag{20}$$

It is desirable to express the above relationship as a function of time by assuming that the sensor is moving parallel to the target surface and with a constant velocity, that is

$$G_i'(t,\Delta f) = G(t) \circledast h_i(t,\Delta f) \tag{21}$$

The total energy contained in this image is given by

$$E_i = \int G_i'(t,\Delta f)\ G_i'^{*}(t,\Delta f)\ dt \tag{22}$$

Notice that for simplicity, the integration along the other dimension (range) is not shown. For this band-limited system, E can be viewed as the summation of a countable number of random variables. Therefore, the probability density function (pdf) of E_i approaches a Gaussian distribution when the number of random variables (or the number of resolution elements contained in the image) becomes large. The mean and variance can be shown to be

$$e[E_i(\Delta f)] = \int \left| h_i(t,\Delta f) \right|^2 dt \cdot \int A(t)\ dt \tag{23}$$

$$v[E_i(\Delta f)] = \int \left| h_i(t,\Delta f) \circledast h_i^{*}(t,\Delta f) \right|^2 dt \cdot \int A^2(t)\ dt \tag{24}$$

The proof of the above equations is given in Appendix A. The mean of E_i is simply the product of energy contained in the i-th impulse response and the integral of the reflectivity density.

Statistically, E_i and E_j are independent for $i \neq j$ if the following conditions are satisfied for any positive integer n:

$$e[E_i(\Delta f)\ E_j(\Delta f)^n] = e[E_i^n(\Delta f)]\ e[E_j^n(\Delta f)] \tag{25}$$

D. PDF OF THE NORMALIZED ENERGY DIFFERENCE

Since the arithmetic summation of Gaussian random variables is also a Gaussian random variable, the total energy E_T and energy difference DE also follow Gaussian distribution, with their mean and variance given by the following equations:

$$e[E_T(\Delta f)] = \int \sum_i \left| h_i(t,\Delta f) \right|^2 dt \cdot \int A(t)\ dt \tag{26}$$

$$v[E_T(\Delta f)] = \int \sum_i \left| h_i(t,\Delta f) \ \textcircled{x}\ h_i^*(t,\Delta f) \right|^2 dt \cdot \int A^2(t)\ dt \tag{27}$$

$$e[DE(\Delta f)] = \int \left\{ \sum_{i=1}^{N/2} \left| h_i(t,\Delta f) \right|^2 - \sum_{i=N/2+1}^{N} \left| h_i(t,\Delta f) \right|^2 \right\} dt \cdot \int A(t)\ dt \tag{28}$$

$$v[DE(\Delta f)] = \int \sum_i \left| h_i(t,\Delta f) \ \textcircled{x}\ h_i^*(t,\Delta f) \right|^2 dt \cdot \int A^2(t)\ dt \tag{29}$$

When the processing Doppler centroid approaches to the true Doppler centroid, $e[DE(\Delta f)]$ approaches zero. For images containing a large number of resolution elements, it can be proved that $v[E_T(\Delta f)]/e^2[E_T(\Delta f)]$ is also quite small. Under these two conditions and using the properties of the QHS given

above, the pdf of $\Delta\bar{E}(\Delta f)$ can be accurately modeled by a Gaussian distribution, with its mean and variance given by

$$e[\Delta\bar{E}(\Delta f)] = e[DE(\Delta f)]/e[E_T(\Delta f)] \tag{30}$$

$$v[\Delta\bar{E}(\Delta f)] = v[DE(\Delta f)]/e^2[E_T(\Delta f)] \tag{31}$$

Using Eqs. (15) and (16), the following results can be obtained:

$$e[\Delta\bar{E}(\Delta f)] = \frac{\int_{\frac{-PBW}{2}+\Delta f}^{\Delta f} \hat{W}_a(f)\ df - \int_{\Delta f}^{\frac{PBW}{2}+\Delta f} \hat{W}_a(f)\ df}{\int_{\frac{-PBW}{2}+\Delta f}^{\frac{PBW}{2}+\Delta f} \hat{W}_a(f)\ df} \tag{32}$$

$$v[\Delta\bar{E}(\Delta f)] = \frac{\left\{\int_{\frac{-PBW}{2}+\Delta f}^{\frac{PBW}{2}+\Delta f} \hat{W}_a^2(f)\ df\right\} \cdot \left\{\int A^2(t)\ dt\right\}}{\left\{\int_{\frac{-PBW}{2}+\Delta f}^{\frac{PBW}{2}+\Delta f} \hat{W}_a(f)\ df\right\}^2 \cdot \left\{\int A(t)\ dt\right\}^2} \tag{33}$$

For small Δf, the energy difference between two sides of the antenna pattern is nearly proportional to Δf; therefore, $e[\Delta\bar{E}(\Delta f)]$ can be approximated by

$$e[\Delta\bar{E}(\Delta f)] = C_1 \cdot \Delta f \tag{34}$$

where

$$C_1 = \frac{2\left(\hat{W}_a(0) - \hat{W}_a(PBW/2)\right)}{\int_{\frac{-PBW}{2}}^{\frac{PBW}{2}} \hat{W}_a(f)\ df} \tag{35}$$

C_1 is a measure of the directivity of the antenna pattern. In Eq. (33),

$$\left\{\int \hat{W}_a^2(f)\ df\right\} \Big/ \left\{\int \hat{W}_a(f)\ df\right\}^2$$

is a measure of the time-resolution constant [13]. Hence, it can be represented by the product of a constant, C_2, and 1/PBW in cases where Δf is much smaller than PBW. Also, we may define the contrast of the target-reflectivity profile to be

$$\rho = \frac{\frac{1}{T_a}\int A^2(t)\ dt}{\left\{\frac{1}{T_a}\int A(t)\ dt\right\}^2} - 1 \tag{36}$$

Thus, $v[\Delta\bar{E}(\Delta f)]$ can be expressed as

$$v[\Delta\bar{E}(\Delta f)] = C_2(\rho + 1)/(PBW \cdot T_a) = C_2(\rho + 1)/N_s \tag{37}$$

where T_a is the time corresponding to the size of the image along the azimuth and N_s is defined as the total number of resolution elements of the image.

E. STANDARD DEVIATION OF THE DOPPLER CENTROID ESTIMATE

From the statistical properties of $\Delta\bar{E}(\Delta f)$ given above, we can form the joint pdf of Δf and $\Delta\bar{E}$ as follows:

$$p(\Delta f, \Delta\bar{E}) = \frac{1/DF}{C_0 \left(2\pi C_2(\rho + 1)/N_s\right)^{1/2}} \exp \left\{\frac{-(\Delta\bar{E} - C_1\Delta f)^2}{2C_2(\rho + 1)/N_s}\right\}$$

$$\text{for } |\Delta f| \leq DF/2, \quad |\Delta\bar{E}| \leq 1 \tag{38}$$

where DF is chosen such that Eq. (37) is satisfied. C_0 is determined from the condition $\iint p(\Delta f, \Delta\bar{E}) \cdot d\Delta f \cdot d\Delta\bar{E} = 1$. The contour plot of this pdf is shown in Figure 3. The Doppler centroid is determined with the criterion $\Delta\bar{E} = 0$. Therefore, the distribution of error of the Doppler centroid estimate is given by the conditional pdf $p(\Delta f/\Delta\bar{E} = 0)$ where

$$p(\Delta f/\Delta\bar{E} = 0) = p(\Delta f, \Delta\bar{E})/p(\Delta\bar{E} = 0) \tag{39}$$

An analytical expression for $p(\Delta\bar{E} = 0)$ is generally difficult to obtain. However, when N_s is large enough such that $p(DF/2, \Delta\bar{E} = 0)$ approaches zero, we may find that $C_0 = 1$ and

$$p(\Delta\bar{E} = 0) = 1/(DF \cdot C_1) \tag{40}$$

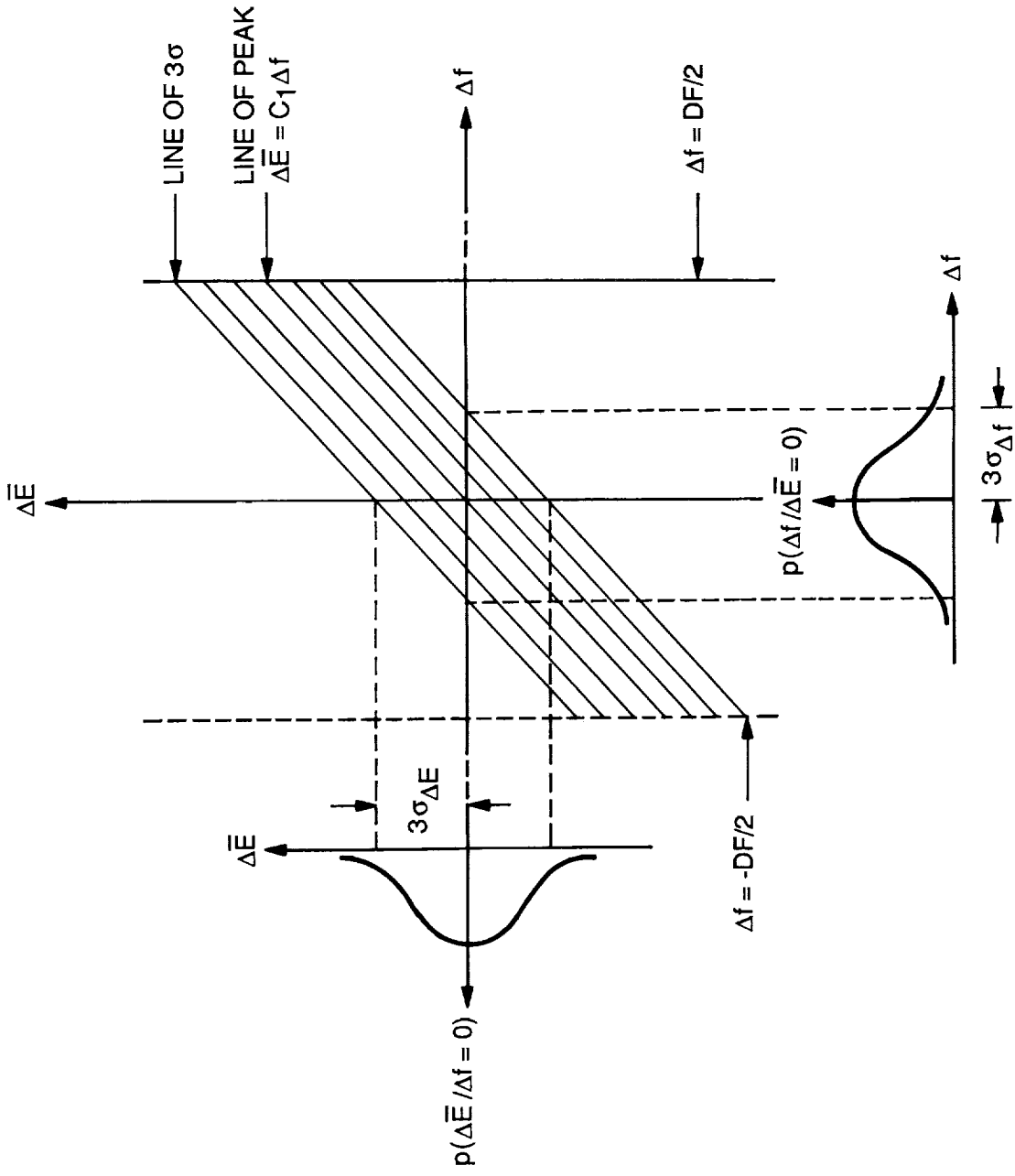

Figure 3. Contours and Projections of $p(\Delta f, \Delta\bar{E})$

Finally, the pdf of the Doppler centroid estimation error is given by

$$p(\Delta f/\Delta\bar{E} = 0) = \frac{C_1}{\left(2\pi C_2(\rho + 1)/N_s\right)^{1/2}} \exp\left\{\frac{-(C_1 \cdot \Delta f)^2}{2C_2(\rho + 1)/N_s}\right\} \tag{41}$$

The Doppler centroid estimate is unbiased, and its standard deviation can be shown to be $(C_2(\rho + 1)/N_s)^{1/2}/C_1$ under the conditions given above.

F. AZIMUTH AMBIGUITY EFFECT

Another possible source of error in the Doppler centroid estimate is due to the azimuth ambiguity, which is caused by aliasing resulting from the limited pulse repetition frequency (PRF) employed by most radar [14]. The effect of the azimuth ambiguity on an SAR image is that a "ghost image" of the terrain outside of the beamwidth of the antenna mainlobe would be superimposed onto the image of the terrain within the mainlobe.

By including the azimuth ambiguity effect, the mean and variance of the normalized energy difference are given by

$$e[\Delta\bar{E}(\Delta f)] = \frac{\sum_k \left\{\int_{f_1(k)}^{f_2(k)} \hat{W}_a(f)\, df \cdot \int_{t_{\ell k}} A(t)\, dt - \int_{f_2(k)}^{f_3(k)} \hat{W}_a(f)\, df \cdot \int_{T_{rk}} A(t)\, dt\right\}}{\sum_k \left\{\int_{f_1(k)}^{f_3(k)} \hat{W}_a(f)\, df \cdot \int_{T_k} A(t)\, dt\right\}} \tag{42}$$

$$v[\Delta\bar{E}(\Delta f)] = \frac{\sum_k \left\{ \int_{f_1(k)}^{f_3(k)} \hat{W}_a^2(f)\, df \cdot \int_{T_k} A^2(t)\, dt \right\}}{\sum_k \left\{ \int_{f_1(k)}^{f_3(k)} \hat{W}_a(f)\, df \cdot \int_{T_k} A(t)\, dt \right\}^2} \tag{43}$$

where

$$f_1(k) = \Delta f + kPRF - PBW/2$$

$$f_2(k) = \Delta f + kPRF$$

$$f_3(k) = \Delta f + kPRF + PBW/2 \tag{44}$$

The terms T_k, $T_{\ell k}$, and T_{rk} are the domains of integration for targets which are associated with Doppler frequencies between $f_1(k)$ and $f_3(k)$, $f_1(k)$ and $f_2(k)$, and $f_2(k)$ and $f_3(k)$, respectively.

The mean of the normalized energy difference is not very sensitive to the error of the processing Doppler because of the ambiguity effect. There is very little change to the magnitude of $v[\Delta\bar{E}(\Delta f)]$. This effect leads to an increase in the standard deviation of the Doppler centroid estimate. However, the azimuth ambiguity is generally reduced by selecting a reasonably large PRF. In such cases, its effect on the Doppler centroid estimate is not significant and can be neglected.

G. SYSTEM-NOISE EFFECT ON DOPPLER ESTIMATION

The previous sections did not treat the effect of SAR system noise on the DCE process. There are several types of noise sources in the SAR system: noise from the atmosphere, noise contributed by the receiver, and the quantization noise. If we assume that these noise sources are additive, the single-look SAR image can be expressed as

$$G_i'(t) = G(t) \circledast h_i(t) + n(t) \tag{45}$$

The bandwidth of n(t) is limited by the bandwidth of the correlator. Assume that n(t) is a Gaussian complex process with independent quadrature components and is uncorrelated with X(t). The mean and variance of the normalized energy difference can be found to be

$$e[\Delta\bar{E}(\Delta f)] = C_1 \Delta f/(1 + 1/SNR) \tag{46}$$

$$v[\Delta\bar{E}(\Delta f)] = \frac{C_2(\rho + 1) + 2/SNR + 1/SNR^2}{N_s(1 + 1/SNR)^2} \tag{47}$$

The standard deviation of the Doppler centroid estimate is given by $[(C_2(\rho + 1) + 2\ SNR^{-1} + SNR^{-2})/N_s]^{1/2}/C_1$. The error of the Doppler centroid estimate decreases when any of the following occur:

(1) the number of resolution elements (N_s) increases

(2) the signal-to-noise ratio (SNR) increases

(3) the antenna directivity (C_1) increases

(4) the reflectivity contrast (ρ) decreases

SECTION IV

EXPERIMENTAL RESULTS: GENERALIZED DCE ALGORITHM

The generalized DCE algorithm, implemented with four looks, was applied to several Seasat and SIR-B data sets. The standard deviation of the estimated Doppler centroid was calculated by using the same technique originally described by Li [1]. A SAR data set with a size capable of producing a 1k (range) x 4k (azimuth) pixel (full-resolution, slightly oversampled) image is processed to obtain 16 Doppler centroid estimates which correspond to spatially consecutive image blocks having 64k (range) x 4k (azimuth) pixels. These Doppler estimates are fitted by a linear function of the range. The root-mean-square deviation from the linear fit is taken to be the standard deviation of the Doppler centroid estimate. This method is valid because the actual Doppler centroid can be accurately approximated by a linear function of the range for both the Seasat and the SIR-B cases. The standard deviations of the Doppler centroid estimates from several data sets are tabulated in Table I. The predicted standard deviations of the Doppler centroid estimates and the contrasts of the reflectivity profile of the source are also listed in Table I.

These reflectivity-contrast values are measured from the full-resolution image data by using the method described below. It is well known that the observed intensity of each full-resolution image pixel is the product of the local reflectivity of the source and a random speckle noise with an exponential distribution. If we assume that the reflectivity of the source and the

Table I. Results of DCE Algorithm III and Prediction

DATA SET	SCENE CONTENT	$\sigma_{f_{dc}}$		$\rho + 1$
		ESTIMATION	PREDICTION	
SEASAT REV. 1183 GULF OF CALIFORNIA	UNIFORM ROUGH OCEAN SURFACE	1.5 (Hz)	1.4	1.02
SEASAT REV. 762	PERIODIC OCEAN WAVES	2.0	1.8	1.6
SEASAT REV. 1254 GARDEN CITY, KANSAS	AGRICULTURE FIELD	2.7	2.4	3.0
SEASAT REV. 351 SAN GABRIEL MTNS.	MOUNTAINS	4.1	2.8	4.2
SEASAT REV. 351 L.A. AIRPORT, CALIF.	AIRPORT IN URBAN AREA	8.1	3.7	7.3
SIR-B REV. 6 W. MONTREAL, QUEBEC	URBAN AREA	10.4	4.6	11.2

random speckle noise are independent, the contrast of the source reflectivity is given by

$$\rho = \frac{M_2}{2M_1} - 1 \tag{48}$$

where M_1 is the mean pixel intensity and M_2 is the mean squared pixel intensity. The antenna directivity constant C_1 and the effective bandwidth constant C_2 are calculated based on the given antenna pattern [15].

Table I shows that the predicted Doppler centroids are very close to the Doppler centroids estimated from the SAR data for a uniform ocean surface, periodic ocean waves, and agriculture fields. This indicates that the performance analysis given in Section II does apply well to the QHS. Table I also shows that large differences between predictions and estimates exist for the mountain and urban sources. This indicates that these sources are not accurately modeled by a QHS. However, the prediction does provide an indication of the growth of estimation errors for these cases.

SECTION V

OPTIMAL DOPPLER CENTROID ESTIMATION FOR QHS

The DCE algorithms described above do not yield an optimal Doppler centroid estimate for a QHS. This fact is illustrated by the following example. Consider a source consisting of two equal areas, each of which has a uniform reflectivity and a very large signal-to-noise ratio. Assume that the reflectivity level of one area is much greater than the other. The errors of the Doppler centroid estimates obtained from each individual area are almost equal; therefore, arithmetic averaging reduces the estimation error by a factor of $1/\sqrt{2}$. However, the error of the Doppler centroid estimate obtained by applying those algorithms described in Section IIB over the entire area would be almost equal to those from each individual area.

In the above example, the greater uncertainty contained in the Doppler centroid estimate from those algorithms is due to the fact that the weight is given by the percentage of energy contained in each subarea instead of by the size of each subarea. This can be seen from the following expression for $\Delta\bar{E}$:

$$\Delta\bar{E} = \Delta\bar{E}(1)\,\frac{E_T(1)}{E_T} + \Delta\bar{E}(2)\,\frac{E_T(2)}{E_T} \tag{49}$$

where $\Delta\bar{E}(1)$ and $\Delta\bar{E}(2)$ stand for the normalized energies corresponding to those subareas, and $E_T(1)$ and $E_T(2)$ are the total energies corresponding to those subareas.

The above example also gives a hint for an optimal approach. A QHS can be thought of as a source consisting of a set of spatially segregated subsources, each of which is a homogeneous source. The first step of an optimal DCE process for a QHS (also called an optimal QHS-DCE process) is to obtain a set of optimal Doppler centroid estimates from these subsources. The next step is to obtain a final estimate based on these preliminary results. The solution for the second step is quite obvious. An optimal Doppler centroid estimate based on the maximum likelihood criterion is given by the weighted sum of those preliminary estimates, where each weight coefficient is inversely proportional to the variance of each preliminary estimate. Let $\sigma_{f_{dc}}(k)$ be the standard deviation of the Doppler centroid estimate of the k-th subsource. The associated weight coefficient to be used in the optimal QHS-DCE process is given by

$$W_c(k) = \frac{\sigma_{f_{dc}}^{-2}(k)}{\sum_{k=1}^{K} \sigma_{f_{dc}}^{-2}(k)} \tag{50}$$

The standard deviation of the final Doppler centroid estimate is given by

$$\sigma_{f_{dc}} = \left(\sum_{k=1}^{K} W_c^2(k) \; \sigma_{f_{dc}}^2(k) \right)^{1/2}$$

$$= \left(\sum_{k=1}^{K} \sigma_{f_{dc}}^{-2}(k) \right)^{-1/2} \tag{51}$$

The optimal homogeneous-source DCE algorithm using a linear estimation approach has been developed and will be reported in another publication [16]. The detailed analysis of this algorithm will not be repeated here. However, an introduction to the problem and the optimization analysis involved are given in Appendix B. In the following we describe the processing procedures, which include both time domain and frequency domain approaches. The time domain approach can be incorporated in the optimal QHS-DCE process more easily than the frequency domain approach.

A. OPTIMAL DOPPLER CENTROID ESTIMATION FOR HS

The frequency domain approach is used to obtain the range-averaged power density spectrum from a full-resolution image. The next step is to convolve this spectrum with $\hat{W}_a'(f)/\hat{W}_a^2(f)$, where $\hat{W}_a'(f)$ is the derivative of $\hat{W}_a(f)$ with respect to f. After convolution, the frequency associated with a sample, having its value closest to zero, is the Doppler centroid estimate.

The time domain approach is to process the SAR echo response into N independent single-look images, each with 1/N of the total processing bandwidth, where N is an even number. These single-look images are weighted in the frequency domain with $\hat{W}_a'(f)/\hat{W}_a^2(f)$, by incorporating this weight function in the reference function. Compute $\Delta\bar{E}$ according to Eq. (4). The Doppler centroid estimate is then obtained by subtracting the estimated processing Doppler error $\Delta_{f_{dc}}$ (given in Eq. (52)) from the processing Doppler. Repeat this procedure until $\Delta\bar{E}$ approaches zero. The estimated processing Doppler error is given by

$$\Delta f_{dc} = \frac{\displaystyle\int_{\frac{-PBW}{2}}^{\frac{PBW}{2}} \frac{\left|\hat{W}_a'(f)\right|}{\hat{W}_a(f)}\, df}{\displaystyle\int_{\frac{-PBW}{2}}^{\frac{PBW}{2}} \left(\frac{\hat{W}_a'(f)}{\hat{W}_a(f)}\right)^2 df} \cdot \Delta\bar{E} \tag{52}$$

The standard deviation of the Doppler centroid estimate obtained from this algorithm is given by

$$\sigma_{f_{dc}} = \frac{\left(\displaystyle\int_{\frac{-PBW}{2}}^{\frac{PBW}{2}} \left(\frac{\hat{W}_a'(f)}{\hat{W}_a(f)}\right)^2 df/PBW\right)^{-1/2}}{N_s^{1/2}} \cdot f(SNR) \tag{53}$$

The polynomial function f(SNR) is determined by the numerical analysis method. For a large SNR, the value of f(SNR) is equal to one.

In the implementation of the optimal QHS-DCE algorithm, determination of subsource boundaries is not necessary. A simple method is to use the intensity histogram of the multi-look image. The procedure includes the following: Perform multi-look summation to generate the N-look image (to reduce speckle uncertainty) and its histogram. Divide the intensity range, covering more than 99% of the total image pixels, into K intensity intervals. Preliminary Doppler centroid estimates are then obtained from subsets of pixels having the same intensity level. A detailed block diagram of this optimal QHS-DCE process is illustrated in Figure 4.

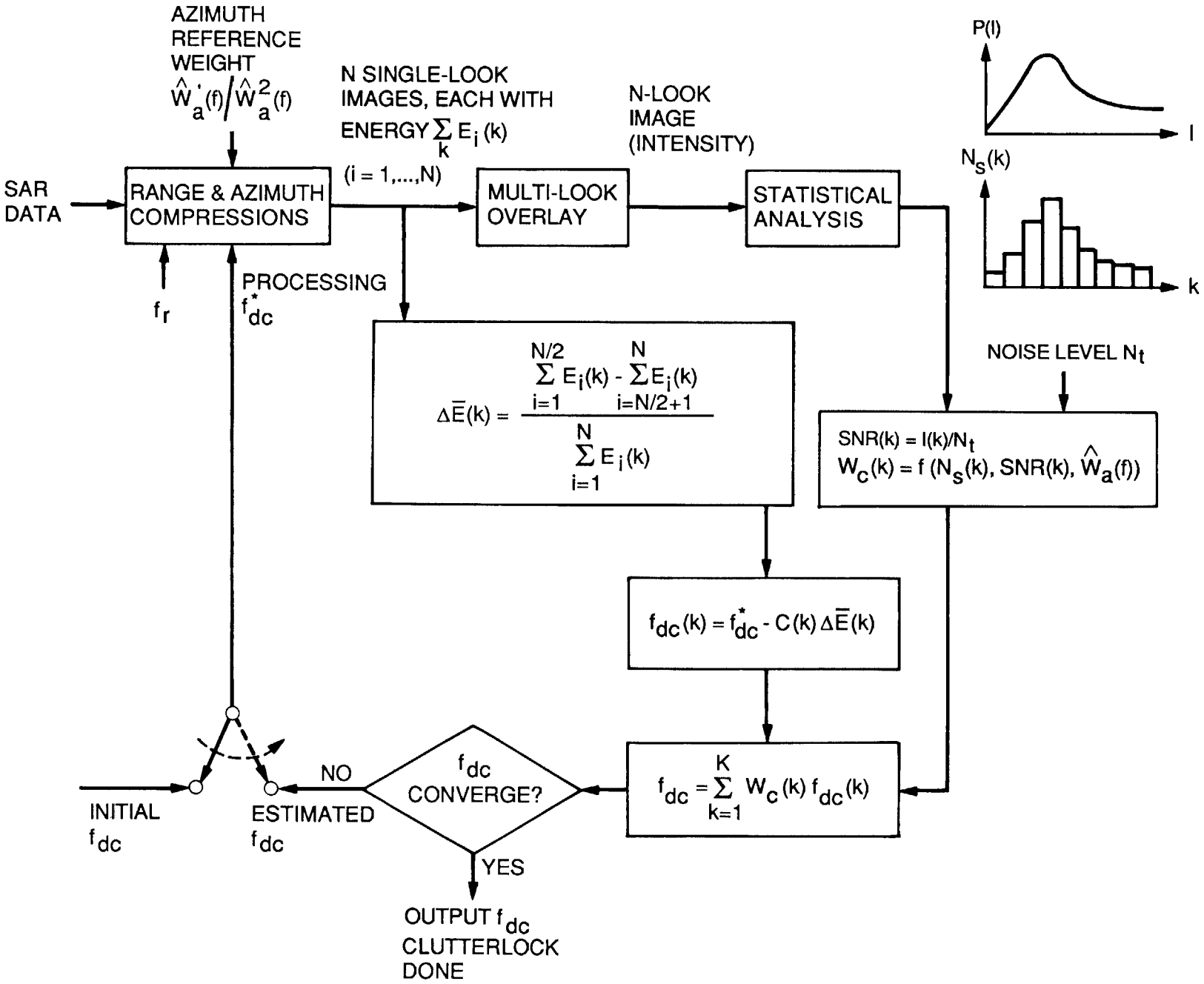

Figure 4. Block Diagram of an Optimal QHS-DCE Algorithm

SECTION VI

EXPERIMENTAL RESULTS: OPTIMAL QHS-DCE ALGORITHM

The optimal QHS-DCE algorithm was applied to the same SAR data sets listed in Table I. The same linear-fit method was used to estimate the standard deviation of the Doppler centroid estimate. Results are listed in Table II. In these cases, the center portions of the linear-fitted lines obtained from both algorithms differ by an amount much smaller than the standard deviation listed in Table II. An improvement of the estimation accuracy can be seen in all the cases, even in urban and mountain sources.

However, for urban and mountain sources, the Doppler centroid estimates are not as accurate as those obtained from the ocean and agriculture areas. This could be due to the fact that the reflectivity profiles of these sources contain high-frequency variations, which are beyond the assumptions of a QHS. Also, the assumption of phase independency among numerous small scatterers may not be true for the urban sources. It is believed that these factors degrade the accuracy of the Doppler centroid estimates.

Table II. Results of an Optimal QHS-DCE Algorithm

DATA SET	SCENE CONTENT	$\sigma_{f_{dc}}$	
		ALGO. III	OPTIMAL
SEASAT REV. 1183 GULF OF CALIFORNIA	UNIFORM ROUGH OCEAN SURFACE	1.5 (Hz)	1.0
SEASAT REV. 762	PERIODIC OCEAN WAVES	2.0	1.2
SEASAT REV. 1254 GARDEN CITY, KANSAS	AGRICULTURE FIELD	2.7	1.5
SEASAT REV. 351 SAN GABRIEL MOUNTAINS	MOUNTAINS	4.1	2.8
SEASAT REV. 351 L.A. AIRPORT, CALIF.	AIRPORT IN URBAN AREA	8.1	3.3
SIR-B REV. 6 W. MONTREAL, QUEBEC	URBAN AREA	10.4	5.5

SECTION VII

CONCLUSION

We have presented a DCE algorithm which is generalized from previously reported algorithms. Detailed performance analysis was given and validated by the experimental results. This performance analysis is directly applicable to Li's algorithm. In Curlander's algorithm, the Doppler centroid estimate can be slightly more accurate when the selected processing Doppler values cover a wide range (to increase the effective total number of resolution elements) and the azimuth ambiguity levels contributed from two sides of the main targets still balance well.

In the second part of this publication, an optimal DCE algorithm for the quasi-homogeneous source was presented. Experimental results show that it does improve the accuracy of the Doppler centroid estimates for all the tested data sets.

APPENDIX A

PROOF OF (23) AND PROOF OF (24)

A. PROOF OF (23)

From Eqs. (21) and (22), the mean of $E_i(\Delta f)$ can be expressed by

$$e[E_i(\Delta f)] = \iiint e[G(t')G^*(t")]h_i(t - t',\Delta f) \; h_i^*(t - t",\Delta f)\, dtdt'dt" \tag{A1}$$

By use of Eqs. (17) and (18), it can be shown that

$$e[G(t')G^*(t")] = A^{1/2}(t')A^{1/2}(t")\delta(t' - t") \tag{A2}$$

Substituting (A2) in (A1), we have

$$e[E_i(\Delta f)] = \iint \left| h_i(t - t',\Delta f) \right|^2 A(t')dt'dt \tag{A3}$$

In (A3), $h_i(t - t',\Delta f)$ can be viewed as a delta function because of the assumption that $A(t')$ is a slowly varying function. This implies

$$e[E_i(\Delta f)] = \int \left| h_i(t,\Delta f) \right|^2 dt \cdot \int A(t)dt \tag{A4}$$

B. PROOF OF (24)

From Eqs. (21) and (22), the mean of $E_i^2(\Delta f)$ can be expressed by

$$e[E_i^2(\Delta f)] = \int \cdots \int e[G(t_1)G^*(t_2)G(t_3)G^*(t_4)]$$

$$\times h_i(t - t_1, \Delta f) h_i^*(t - t_2, \Delta f)$$

$$h_i(t' - t_3, \Delta f) h_i^*(t' - t_4, \Delta f)$$

$$dtdt'dt_1dt_2dt_3dt_4 \qquad \text{(A5)}$$

By use of (17) and (18), it can be shown that

$$e[G(t_1)G^*(t_2)G(t_3)G^*(t_4)] = A^{1/2}(t_1)A^{1/2}(t_2)A^{1/2}(t_3)A^{1/2}(t_4)$$

$$[\delta(t_1 - t_2)\delta(t_3 - t_4) + \delta(t_1 - t_4)\delta(t_2 - t_3)] \qquad \text{(A6)}$$

Substituting (A6) in (A5), we have

$$e[E_i^2(\Delta f)] = e^2[E_i(\Delta f)]$$

$$+ \int\int \left| h_i(t_1 - t_2, \Delta f) \circledast h_i^*(t_1 - t_2, \Delta f) \right|^2 A(t_1)A(t_2)dt_1dt_2$$

(A7)

In (A7), $h_i \circledast h_i^*$ can be viewed as a delta function because of the assumption that A(t') is a slowly varying function. This implies

$$v[E_i(\Delta f)] = \int \left| h_i(t,\Delta f) \circledast {}^{*}_{i}(t,\Delta f) \right|^2 dt \cdot \int A^2(t)dt \qquad \text{(A8)}$$

APPENDIX B

OPTIMAL DOPPLER CENTROID ESTIMATION FOR HS

The spectrum of the SAR response from a homogeneous source can be expressed by the following function:

$$S(f) = p\hat{W}(f - f_{dc})\ \hat{X}(f)\hat{X}^*(f) \tag{B1}$$

where p is proportional to the power of the response and $\hat{X}(f)$ is the Fourier transform of random process X(t) in Eq. (17). $\hat{X}(f)$ can be shown to be a zero-mean complex Gaussian random process with independent quadrature components. The second and fourth moments of $\hat{X}$ are of the same form as those of Eqs. (18) and (19). $\hat{W}(f - f_{dc})$ is equal to the antenna pattern $\hat{W}_a(f)$ given in Eq. (9).

The Doppler centroid estimate from a linear estimator can be expressed by

$$\hat{f}_{dc}(f_1) = f_1 + \hat{\Delta f}(f_1) \tag{B2}$$

where

$$\hat{\Delta f}(f_1) = \int_{f_1-F/2}^{f_1+F/2} S(f)g(f - f_1)\ df \tag{B3}$$

Here, $g(f)$ is the weight function; f_1 is the frequency reference of $g(f)$. F is the frequency bandwidth over which the estimation is performed. The mean and variance of $\hat{\Delta f}(f_1)$ can be expressed by the following equations when f_1 approaches f_{dc}.

$$e[\hat{\Delta f}(f_1)] \cong P \int_{-F/2}^{F/2} \hat{W}(f)g(f)\ df + (f_1 - f_{dc}) \cdot P \int_{-F/2}^{F/2} \hat{W}'(f)g(f)\ df \qquad (B4)$$

and

$$v[\hat{\Delta f}(f_1)] \cong P^2 \int_{-F/2}^{F/2} \hat{W}^2(f)g^2(f)\ df \qquad (B5)$$

Here, we shall find a function for $g(f)$ which yields an unbiased and optimal estimate of f_{dc}. The "optimal" estimate is interpreted here as the one having the least mean-square error. Therefore, $g(f)$ must minimize $v[\Delta f(f_1)]$ and satisfy the following:

$$\int_{-F/2}^{F/2} \hat{W}(f)g(f)\ df = 0 \qquad (B6)$$

$$P \int_{-F/2}^{F/2} \hat{W}'(f)g(f)\ df = 1 \qquad (B7)$$

Let $g(f) = C\ g_1(f)\ g_2(f)$, and solve for C from Eq. (B7). Substituting C in Eq. (B5), the problem becomes one of maximizing

$$\frac{\left\{\int_{-F/2}^{F/2} \hat{W}'(f) g_1(f) g_2(f)\ df\right\}^2}{\int_{-F/2}^{F/2} \hat{W}^2(f) g_1^2(f) g_2^2(f)\ df} \tag{B8}$$

By choosing $g_1(f)$ to be equal to $1/\hat{W}(f)$ and using the Cauchy-Schwarz Inequality, we can show that the solution for $g_2(f)$ is the function $\hat{W}'(f)/\hat{W}(f)$. Hence the weight function $g(f)$ is given by

$$g(f) = \frac{1}{P\int_{-F/2}^{F/2} \left(\frac{\hat{W}'(f)}{\hat{W}(f)}\right)^2 df} \cdot \frac{\hat{W}'(f)}{\hat{W}^2(f)} \tag{B9}$$

For a conventional SAR antenna pattern, $\hat{W}(.)$ is symmetric and its first-order derivative is asymmetric, i.e.,

$$\hat{W}'(f) = -\hat{W}'(-f) \tag{B10}$$

This implies that $g(f)$ is also asymmetric and satisfies (B6).

APPENDIX C

REFERENCES

1. Li, F.K., Held, D.N., Curlander, J., and Wu, C., Doppler Parameter Estimation for Synthetic Aperture Radars. IEEE Transactions on Geoscience and Remote Sensing. Vol. GE-23, No. 1, January, 1985.

2. Gonzalez, F.I., Rufenbach, C.L., and Shuchman, R.A., Surface Current Detection Using SAR Data, Proc. of the COSPAR/SCOR/IUCRM Symposium on Oceanography from Space, 1981.

3. Shuchman, R.A., Rufenbach, C.L., Gonzalez, F.I., and Klooster, A., The feasibility of measurement of ocean surface currents using Synthetic Aperture Radars, in Proc. 13th Int. Symp. Remote Sensing Environment (Ann Arbor, MI), pp. 93-103, 1979.

4. Wu, C., Curlander, J.C., and DiCenzo, A., Determination of Spacecraft Attitude Using Synthetic Aperture Radar Data, AIAA Sensor Systems for the 80's Conference, Colorado Springs, Dec. 2-4, 1980.

5. Wu, C., Liu, K.Y., and Jin, M.Y., Modeling and a Correlation Algorithm for Spaceborne SAR Signals, IEEE Trans. on Aerosp. Electron. Syst., Vol. AES-18, No. 5, September 1982, pp. 563-575.

6. Curlander, J., Wu, C., Li, F.K., and Held, D.N., Estimation of Doppler Parameters for Spaceborne Synthetic Aperture Radar Processing (in preparation).

7. Cumming, I.G., and Bennet, J.R., Digital Processing of SEASAT SAR Data, International Conference on Acoustics, Speech and Signal Processing, Washington, D.C., Apr. 1979.

8. Porcello, L.J., Massey, N.G., Innes, R.B., and Marks, J.M., Speckle Reduction in Synthetic-Aperture Radars, Journal of the Opt. Soc. of Amer., Vol. 66, No. 11, Nov. 1976, pp. 1305-1311.

9. Kondo, K., Ichioka, Y., and Suzuki, T., Image Restoration by Wiener Filtering in the Presence of Signal-Dependent Noise, Applied Optics, Sept. 1977, 16, pp. 2554-2558.

10. Frost, V.S., Stiles, J.A., Shanmugam, K.S., Holtzman, J.C., and Smith, S.A., An Adaptive Filter for Smoothing Noisy Radar Images, Proceedings of the IEEE, Jan. 1981, 69, pp. 133-135.

11. Carter, W.H., and Wolf, E., Coherence and Radiometry with Quasi-homogeneous Planar Sources, Journal of the Optical Society of America, Vol. 67, No. 6, June 1977, pp. 785-796.

12. Raney, R.K., Transfer Functions for Partially Coherent SAR Systems, IEEE Transactions on Aerospace and Electronic Systems, Vol. AES-19, No. 5, September 1983, pp. 740-750.

13. Deley, G.W., Waveform Design. In Radar Handbook, M. I. Skolnik (Ed.), New York: McGraw-Hill, 1970, Ch. 3, p. 11.

14. Li, F.K., and Johnson, W.T.K., Ambiguities in Spaceborne Synthetic Aperture Radar Systems, IEEE Trans. Aerosp. Electron. Syst., Vol. AES-19, No. 3, pp. 389-397, May 1983.

15. Jordan, R.L., The SEASAT-A Synthetic Aperture Radar System, IEEE Journal of Ocean Engineering, Vol. OE-5, pp. 154-164, April 1980.

16. Jin, M.Y., and Chang, C.Y., Optimal Doppler Centroid Estimation for SAR Data from a Homogeneous Source (submitted to IEEE Transactions on Aerospace and Electronic Systems).